ACS Energy LETTERS

http://pubs.acs.org/journal/aelccp

LETTER

Optical Resonance Engineering for Infrared Colloidal Quantum Dot Photovoltaics

Olivier Ouellette,[†] Nadir Hossain,[†] Brandon R. Sutherland,[†] Amirreza Kiani,[†] F. Pelayo García de Arquer,[†] Hairen Tan,[†] Mohamed Chaker,[‡] Sjoerd Hoogland,[†] and Edward H. Sargent*[,†]

[†]Department of Electrical and Computer Engineering, University of Toronto, 10 King's College Road, Toronto, Ontario M5S 3G4, Canada

[‡]LMN, Institut National de la Recherche Scientifique, 1650 Boulevard Lionel Boulet, Varennes, Québec J3X 1S2, Canada

Supporting Information

ABSTRACT: We report optically enhanced infrared-harvesting colloidal quantum dot solar cells based on integrated Fabry–Perot cavities. By integrating the active layer of the photovoltaic device between two reflective interfaces, we tune its sensitivity in the spectral region at 1100–1350 nm. The top and bottom electrodes also serve as mirrors, converting the device into an optical resonator. The front conductive mirror consists of a dielectric stack of SiN_x and SiO_2 with a terminal layer of ITO and ZnO in which current can flow, while the back mirror consists of a highly reflective gold layer. Adjusting the reflectivity and central wavelength of the front mirror as well as the thickness of the active layer allowed increases in absorption by a total of 56% in the infrared, leading to a record external quantum efficiency of 60% at 1300 nm. This work opens new avenues toward low-cost, high-efficiency rear-junction photovoltaic harvesters that add to the overall performance of silicon solar cells.

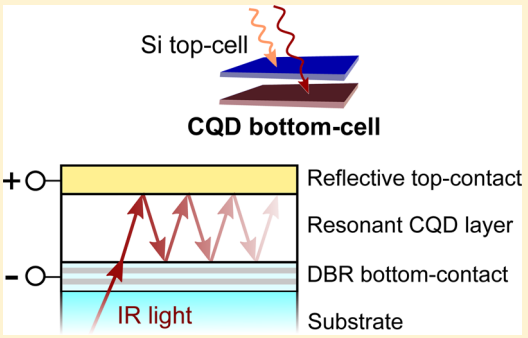

Silicon-based photovoltaics account for ~90% of the world's solar energy production.[1,2] Silicon research includes focus on reducing costs and improving manufacturability;[1,3,4] indeed, silicon solar cells operate impressively close to their theoretical performance limit.[5]

Recent advances in photovoltaic materials include those aimed at improving and complementing the light-harvesting capabilities of silicon via multijunction techniques. Notably, hybrid organic–inorganic perovskites are promising candidates for the front junction,[6,7] whereas colloidal quantum dots (CQDs), if used in a rear-junction device, extend the spectral range of operation of the device further into the infrared.[8]

CQD solids possess a number of benefits, including solution-processing and a readily tunable band gap.[9,10] The latter property allows photovoltaic devices made with this material to harvest solar energy beyond silicon's 1100 nm absorption edge, where more than 15% of the sun's power reaching the earth's surface lies (Figure 1a). Detailed balance considerations show that 0.92 eV constitutes an ideal band gap for a bottom cell. Such a cell collects sunlight between 1100 and 1350 nm and could add up to 6 absolute power points on top of the solar power conversion efficiency (PCE) of silicon solar cells.[11] Current matching between the silicon and CQD cells can be achieved in a four-terminal configuration by adjusting the relative areas of the cells connected in series.[6]

A trade-off is observed in certain thin-film solar cells between light absorption and photoexcited carrier extraction.[8] This is illustrated in Figure 1b, which shows experimentally how the internal quantum efficiency (IQE) in a CQD solar cell decreases with active layer thickness (see the Experimental Methods section). Numerous strategies have been explored to overcome this compromise: plasmonics,[12] subwavelength texturing,[13,14] as well as interference and resonance management.[15−22]

In this work, we present a resonant cavity-enhanced (RCE) optical strategy inspired by previous work in the field of photodetectors[24] that improves the performance of IR CQD solar cells destined to work as the rear junction in a Si/CQD tandem solar cell. This strategy is based on an integrated Fabry–Perot cavity whose resonance is tuned to the spectral region of interest. The optical cavity consists of the quantum dot active layer placed between a dielectric mirror in the front and a reflective gold layer on the back, with each mirror also serving as an electrical contact (Figure 1c). The cavity's resonance wavelength is tuned by adjusting the thickness of the active layer, and its bandwidth is controlled via the reflectivity of the dielectric stack.[25]

The first part of this investigation consisted of finding the optimal combination of front-mirror reflectivity and QD layer

Received: September 1, 2016
Accepted: September 29, 2016

DOI: 10.1021/acsenergylett.6b00403
ACS Energy Lett. 2016, 1, 852–857

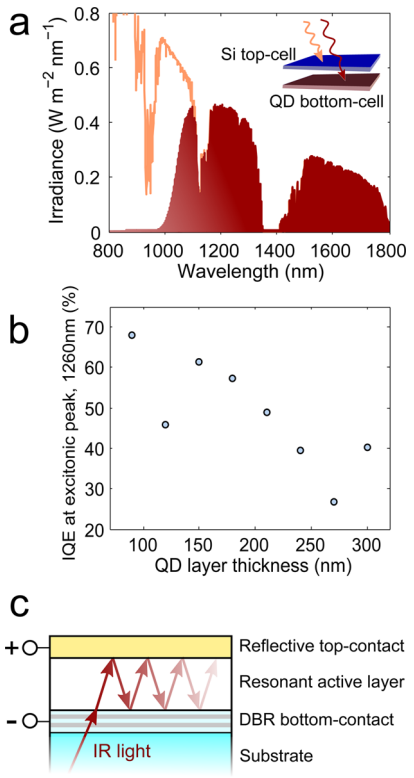

Figure 1. Concept of the cavity-enhanced infrared CQD solar cell. (a) The portion of the AM1.5G sun spectrum to which 500 μm of intrinsic silicon is transparent.[23] More than 15% of the sun's power reaching the earth's surface lies beyond 1100 nm. (b) IQE at the excitonic peak measured for control devices with varying thicknesses. (c) Schematic of the Fabry–Perot cavity IR solar cell.

thickness that would yield the highest effective absorbance in the 1100–1350 nm spectral range. We modeled the photovoltaic device as an asymmetric, absorbing Fabry–Perot cavity (Figure 1c). This simplified model, intended to provide an initial assessment of feasibility, assumes light incidence perpendicular to the surface of the device, planar interfaces between the materials, no light diffusion, and nondispersive media and constant reflectivity between 1100 and 1350 nm. The transmittance T and reflectance R of such a cavity can be calculated as a function of wavelength λ, front-mirror reflection coefficient r_1, and cavity thickness t by evaluating the following expressions, from which the absorption A can be extracted (see the Supporting Information for derivation)

$$R = \left| r_1 + \frac{r_1^2 - 1}{r_1} \frac{x}{1 - x} \right|^2$$

$$T = (1 + (r_1 r_2)^2 - r_1^2 - r_2^2) e^{-2\alpha t} \left| \frac{1}{1 - x} \right|^2$$

$$\text{with } x = r_1 r_2 e^{-i4\pi nt/\lambda - \alpha t} \text{ and } A = 1 - T - R \quad (1)$$

where r_2 is the reflection coefficient of the back mirror, n is the refractive index of the cavity material, and α is its absorption coefficient. The resulting effective absorbance, integrated between 1100 and 1350 nm, is illustrated in Figure 2a. Local maxima can be observed, corresponding to combinations of parameters for which the optical resonance of the cavity is located in the spectral range of interest. An optimal cavity thickness of 110 nm and reflection coefficient of −0.8 yield a theoretical maximal absorbance of 8×10^4 cm^{-1}, which represents a 4-fold improvement over the initial value. The existence of an optimal reflectivity illustrates the trade-off between a resonant absorption increase and bandwidth; a near-unity reflectivity, and therefore a high quality-factor cavity, will enhance the absorption in a range much narrower than the range of interest and thus will lead to overall absorption losses, also apparent in Figure 2a.

With these values in hand, we then designed the front mirror. Silicon nitride (SiN_x) and silicon dioxide (SiO_2) were selected as constituents of the dielectric stack for their availability and suitable contrast between their refractive index (2.1 and 1.5 at 1200 nm, respectively; refractive indices for all materials used herein are given in the Supporting Information). The optical behavior of these multilayer structures was calculated by the transfer matrix (TM) method.[26,27] A quarter-wavelength stack of ($SiN_x|SiO_2|SiN_x$) topped with a quarter-wavelength electrode made of indium tin oxide (ITO) and zinc oxide (ZnO) (see Figure 2c) was found to have a reflectivity close to the calculated ideal, wavelength-independent value of ∼0.64, which corresponds to the norm squared of the reflection coefficient r_1. The calculated reflectivity is shown in Figure 2b (dotted lines). With this stack at the front of the device, a CQD layer thickness of approximately 95 nm was found to yield the highest enhanced calculated absorption, which is shown in Figure 2. We multiplied by the AM1.5G solar spectrum and integrated from 1100 to 1350 nm and found that the total number of photons absorbed in the active CQD layer could increase by as much as 56% with the addition of the designed front mirror compared to a control device without the dielectric stack.

The device fabrication process is illustrated in Figure 3a. First, the $SiN_x|SiO_2$ stacks were fabricated via plasma-enhanced chemical vapor deposition (PECVD) on clean glass substrates (experimental conditions are given in the Experimental Methods section). In order to increase the refractive index of the SiN_x layer to 2.1, we used a SiH_4 to NH_3 gas flow ratio of 1.35.[28,29] In addition, special care was taken to clean the deposition chamber to minimize the inclusion of impurities and ensure a smooth and flat top surface, which in turn reduced the chance of producing electrically shorted devices later in the process. Next, the ITO layer was deposited on top of the structure by sputtering. The optimal substrate temperature to obtain high electrical conductivity and optical transmission in the spectral range of interest was experimentally found to be 400 °C.

Prior to active layer deposition, we cleaned the mirrors sequentially using hydrogen peroxide, acetone, and isopropanol ultrasonic baths for 15 min each to ensure the quality of the surface. ZnO, which serves as an electron acceptor, was then spin-coated onto the ITO surface. Next, the active CQD layer was spin-coated layer-by-layer, followed by solid-state ligand exchange with tetrabutylammonium iodide (TBAI, four layers) and 1,2-ethanedithiol (EDT, one layer). A gold layer was finally thermally evaporated to serve as the hole-collecting contact and back mirror.

The thickness of the CQD layer was controlled by varying the spin speed during deposition. The optimal condition, that which yielded the highest number of photons absorbed, was found by measuring the devices' optical absorption with a UV–vis spectrophotometer, shown in Figure 2d. This corresponds to a CQD layer thickness of approximately 95 nm (measured using scanning electron microscopy; see the Supporting

DOI: 10.1021/acsenergylett.6b00403
ACS Energy Lett. 2016, 1, 852–857

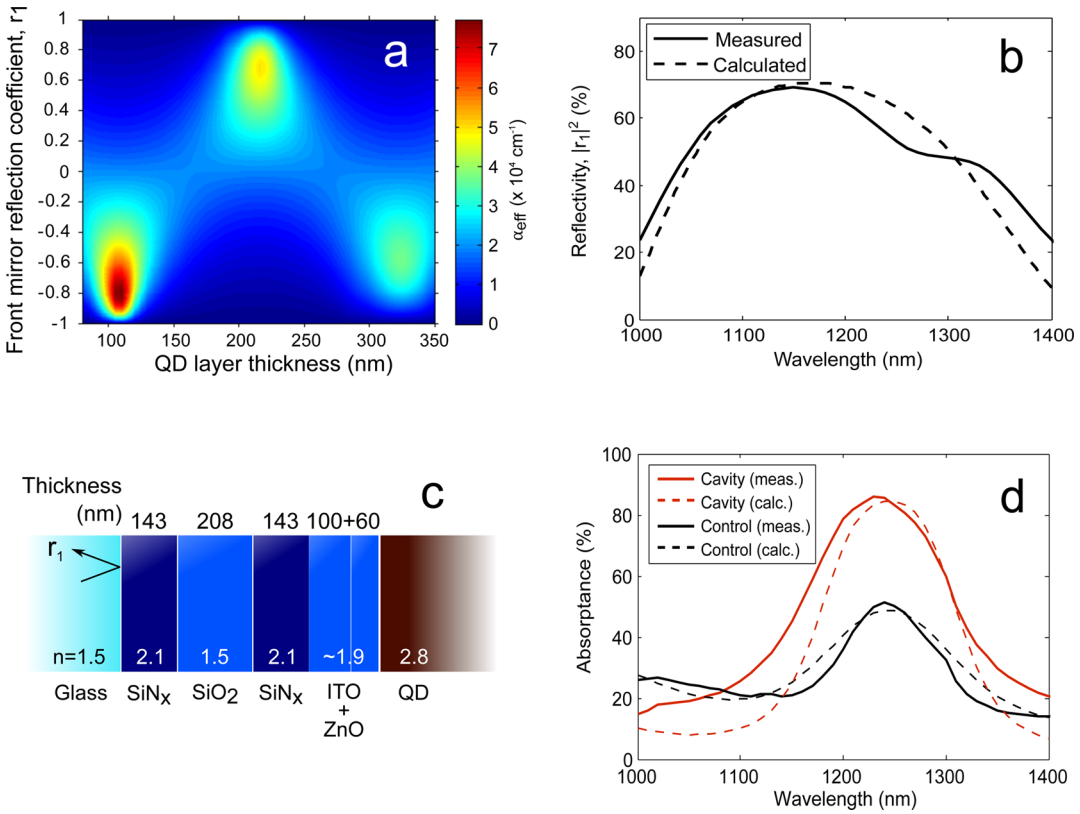

Figure 2. Design of the cavity's front mirror. (a) Calculated effective absorption coefficient (integrated over the 1100−1300 nm range) dependence on mirror reflectivity and cavity length. (b) Reflectivity spectrum of the designed dielectric mirror. (c) Structure of the mirror, showing the thickness and average refractive index of each layer. (d) Absorption spectrum of the control and cavity-based devices.

Information). The measured absorption also features the desired absorption enhancement around the excitonic peak. The UV−vis spectrophotometer was used in reflectance mode to measure the reflectivity of the mirrors as well, shown in Figure 2b. Good agreement is observed between experimental results and calculations, confirming the validity of the design. The differences can be ascribed to slight discrepancies between values used in the model and actual values of refractive indices or layer thicknesses.

Once the devices were fabricated, we proceeded with the characterization of their photovoltaic performance, summarized in Table 1. As expected, the absorption enhancement translates to a notable increase in current density, as is apparent on the devices' current−voltage characteristic under simulated AM1.5 illumination (Figure 3b). The effect of a silicon front cell was replicated with a 1100 nm long-pass filter. A 56% increase in short-circuit current density (J_{sc}) directly leads to an almost identical improvement in PCE, with no notable effect on open-circuit voltage (V_{oc}) and a less than 1% absolute reduction in fill factor (FF). This increase is a close match with the observed absorption enhancement measured previously. The external quantum efficiency (EQE) in Figure 3c shows a record value of 60% at the excitonic peak in the case of the cavity-enhanced device. As is illustrated in Figure 3e, some loss is present below 1160 nm, which is related to the bandwidth/absorption gain compromise mentioned above. These losses can in the future be mitigated with more advanced mirror design and deeper studies of the precise effects of the dielectric stack on the phase of the incident light so that its reflection coefficient r_1 precisely matches the calculated optimal value.

The use of a 1100 nm long-pass filter provides an accurate method for evaluating the performance of the CQD back cell in a real tandem with silicon. In the case of an actual full device, the dielectric mirror would be grown directly on the back of the silicon cell. However, the result illustrated in Figure 2a still holds: a reflection coefficient of approximately −0.8 will still be needed between the CQD active layer and the front stack to obtain resonant absorption enhancement. A slightly modified version of the dielectric stack will therefore have to be designed, taking into account that the substrate this time is silicon rather than glass. Furthermore, the filter that was used has a transmittance that does not exceed 90% above 1100 nm; the device performance that we report therefore takes some actual losses into account.

The spatial distribution of photoexcited carriers in the active layer was also studied. TM calculations[27] further revealed the added advantage of a thinner active layer. As is apparent in Figure 3d, for a thin device, light intensity, and therefore carrier generation, is at its peak near the front ZnO/CQD interface, from which the depletion region originates.[15,30] In contrast, local maxima due to interference caused by reflection at the back mirror[15] are observed deeper in the active layer in the case of a thicker, 300 nm device. Thus, a high proportion of photocarriers generated in these maxima cannot be extracted before recombining, which further contributes to the sharp decrease in the IQE with thickness shown previously in Figure 1b. In addition, when the device operates at its maximum power point (MPP), the depletion region width is reduced, and thus, charge carriers generated far from the ZnO/CQD interface must rely on diffusion rather than drift to be successfully extracted, further reducing the efficiency of the

DOI: 10.1021/acsenergylett.6b00403
ACS Energy Lett. 2016, 1, 852−857

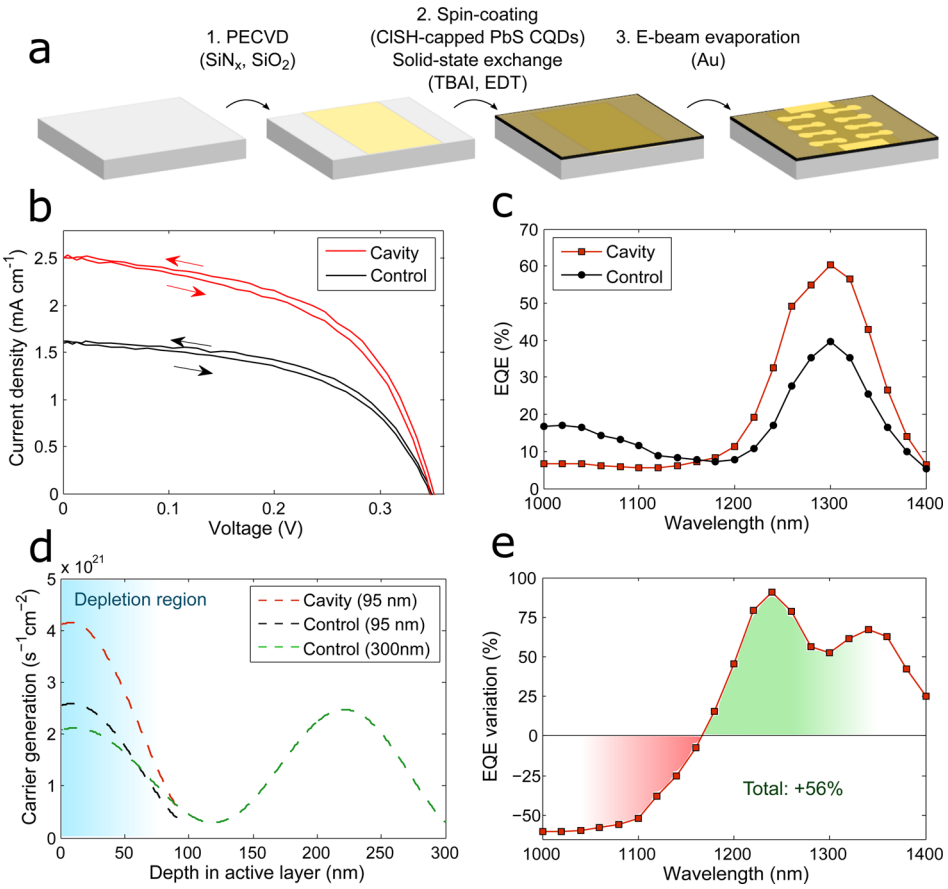

Figure 3. Resonant solar cells' fabrication and performance. (a) Overview of the device fabrication process. (b) Current–voltage (J–V) characteristic of the control and cavity-based devices under a filtered AM1.5 simulated solar spectrum. A 1100 nm long-pass filter was used to replicate silicon. (c) EQE spectrum of both devices. (d) Calculated carrier generation rate distribution in cavity-based and thin (95 nm) and thick (300 nm) control devices. In thinner devices, carriers are generated closer to the depletion region, improving their collection efficiency. (e) Spectral EQE variation of the cavity device over the control, illustrating the overall gain of 56% despite the slightly more narrow-band operation of the cavity-based devices.

Table 1. Open-Circuit Voltage (V_{oc}), Short-Circuit Current Density (J_{sc}), FF, and PCE for a Control and Cavity-Enhanced Device, under Simulated AM1.5 Illumination Passed through a 1100 nm Long-Pass Filter

	V_{oc} (V)	J_{sc} (mA·cm^{-2})	FF (%)	PCE (%)
control	0.35	1.6	55.3	0.31
cavity	0.35	**2.5**	54.4	**0.48**

cell.[31] The optical strategy presented herein therefore possesses the double advantage of increasing light absorption while allowing for an improvement in charge collection.

We have also measured the performance of the devices with varying light incidence angle (see Supporting Information). We found that changes in the absorption profile are negligible up to an incident angle of 20°. For larger angles, the resonance wavelength can be reduced up to 1200 nm. However, the number of photons absorbed is reduced by only 5% at an incident angle of 40°. Therefore, although the use of a sun-tracking apparatus would be desirable, our devices can still perform well even when placed at an angle relative to the sun.

In summary, we demonstrated the successful enhancement of infrared radiation absorption in the active layer of a CQD solar cell intended as the rear junction of a four-terminal Si/CQD tandem cell. We converted the device into an optical resonator through the addition of a dielectric mirror between the glass substrate and the active layer. A 56% increase in IR PCE was achieved by engineering the reflectivity of the front mirror as well as the thickness of the active layer. Performance can be improved by further optimizing the front mirror with special attention given to the phase change from reflections on the dielectric stack. This work also highlights the importance of considering interference effects when designing and fabricating thin-film solar cells as they can greatly influence performance. Once the stability and quality of thin-film photovoltaic materials are further improved, the approach used herein will provide an important tool to bring device performance closer to a successful combination with silicon solar cells.

EXPERIMENTAL METHODS

PbS CQD Synthesis. We followed the synthetic protocol previously reported by Hines[32] with the following modifications to obtain a band gap between 1200 and 1300 nm: 1.8 g of PbO, 6.0 mL of oleic acid, and 27 mL of 1-octadecene (ODE) were loaded in a 250 mL round-bottom three-neck flask, and the mixture was pumped at 100 °C for 60 min. After the solution turned optically clear, the temperature was set to the reaction temperature, ranging from 120 to 135 °C. Hexamethyldisilathiane (TMS) solution in ODE (210 μL in 10 mL of ODE) was rapidly injected into the reaction flask. The heating mantle was turned off but was not removed to provide slow cooling. The

DOI: 10.1021/acsenergylett.6b00403
ACS Energy Lett. 2016, 1, 852–857

dots were isolated by addition of 25 mL of acetone and redispersed in anhydrous toluene. A halide treatment was then performed as reported elsewhere.[31] Prior to deposition, dots were washed in methanol and redispersed in octane at a concentration of 50 mg/mL.

Mirror Fabrication. SiN_x and SiO_2 were deposited using an Oxford plasma-enhanced chemical vapor deposition (PECVD) system. SiO_2 was deposited using a flow rate of N_2O at 710 sccm, 100% Si_3N_4 at 8.5 sccm, and N_2 at 161.5 sccm, at a pressure of 500 mT. SiN_x was deposited using a flow rate of N_2 at 380 sccm, NH_3 at 20 sccm, and 100% SiH_4 at 20 sccm, at a pressure of 1000 mT. In both cases, the substrate temperature was 390 °C. ITO was then deposited using a commercial K. J. Lesker In/Sn (90:10) target in a K. J. Lesker CMS-18 sputtering system. The target was sputtered using an RF source operated in argon at a power of 150 W. The total pressure in the chamber during deposition was maintained at 4 mTorr by automatically adjusting the total flow of the gas in the chamber while putting the gateway valve to "throttle" position. Deposition was performed at a substrate temperature of 400 °C.

Solar Cell Fabrication. Mirror substrates were cleaned with sequential hydrogen peroxide, acetone, and isopropanol ultrasonic baths for 15 min each. One layer of ZnO nanoparticles (synthesized based on previous work[33]) was spin-coated in air at a spin speed of 3000 rpm for 30 s. CQDs were then spin-coated in air as well at 3000 rpm for 10 s, followed by solid-state ligand exchange with tetrabutylammonium iodide (four layers, washed with methanol) and 1,2-ethanedithiol (one layer, washed with acetonitrile). Devices were left to dry for 24 h in air. Then, 120 nm of gold was thermally evaporated by e-beam in an Angstrom Engineering Åmod deposition system in an Innovative Technology glovebox.

Absorptance and Reflectance. Both were measured using a PerkinElmer lambda 950 spectrometer at incident angles of 15 and 8°, respectively. Absorptance was obtained by measuring the total transmittance and reflectance using an integrating sphere and using $A = 1 - T - R$.

AM1.5 Photovoltaic Performance Characterization. Photovoltaic performance under a simulated AM1.5 spectrum was performed as reported previously.[11] Devices were kept in an inert N_2 atmosphere. A Thorlabs 1100 nm long-pass filter was positioned between the source and the device to simulate the effect of a silicon front cell.

External Quantum Efficiency. The EQE was measured using a Stanford Research SR585 current preamplifier and SR830 lock-in amplifier. Monochromatic illumination was provided by a monochromator supplied with a xenon lamp (solar simulator). The light excitation was mechanically modulated at a frequency of 220 Hz. The device was kept in an inert N_2 atmosphere. Spectral measurements (including absorptance) were done without the 1100 nm long-pass filter. They were performed one wavelength step at a time; the use of a filter is therefore not required.

Internal Quantum Efficiency. The IQE was measured on control devices fabricated with the method described above on substrates containing no dielectric stack of $SiN_x|SiO_2$. The EQE and absorptance were measured using the method described above, and the IQE was obtained by dividing the former by the latter. Varying active layer thicknesses were obtained by spin-coating appropriate numbers of layers of CQDs.

Transfer Matrix Calculations. TM calculations were performed using open-source software developed by S. J. Orfanidis, Rutgers University[26] (mirror reflectivity) and by the McGehee group from Stanford University[27] (absorption and carrier generation).

■ ASSOCIATED CONTENT

Supporting Information

The Supporting Information is available free of charge on the ACS Publications website at DOI: 10.1021/acsenergylett.6b00403.

Fabry–Perot model derivation, refractive indices used in calculations, SEM device cross section image, and angular dependence of device absorptance (PDF)

■ AUTHOR INFORMATION

Corresponding Author

*E-mail: ted.sargent@utoronto.ca.

Notes

The authors declare no competing financial interest.

■ ACKNOWLEDGMENTS

The authors thank A. Zitouni, E. Charette, and B. LeDrogoff from the Institut National de la Recherche Scientifique (INRS, Varennes, QC) for support with mirror fabrication, as well as L. Levina, E. Palmiano, D. Kopilovic, and R. Wolowiec for technical support throughout the project. SEM imaging was performed at the Ontario Centre for the Characterisation of Advanced Materials (OCCAM, Toronto, ON). O.O. received financial support from the Fonds de Recherche du Québec – Nature et Technologies (FRQNT). H.T. is financially supported by The Netherlands Organization for Scientific Research (NWO) through a Rubicon grant (680-50-1511).

■ REFERENCES

(1) Jean, J.; Brown, P. R.; Jaffe, R. L.; Buonassisi, T.; Bulović, V. Pathways for solar photovoltaics. *Energy Environ. Sci.* **2015**, *8*, 1200–1219.

(2) Chapin, D. M.; Fuller, C.; Pearson, G. A new silicon p–n junction photocell for converting solar radiation into electrical power. *J. Appl. Phys.* **1954**, *25*, 676–677.

(3) Shi, E.; Li, H.; Yang, L.; Zhang, L.; Li, Z.; Li, P.; Shang, Y.; Wu, S.; Li, X.; Wei, J.; et al. Colloidal antireflection coating improves graphene–silicon solar cells. *Nano Lett.* **2013**, *13*, 1776–1781.

(4) Savin, H.; Repo, P.; von Gastrow, G.; Ortega, P.; Calle, E.; Garín, M.; Alcubilla, R. Black silicon solar cells with interdigitated back-contacts achieve 22.1% efficiency. *Nat. Nanotechnol.* **2015**, *10*, 624–628.

(5) Polman, A.; Knight, M.; Garnett, E. C.; Ehrler, B.; Sinke, W. C. Photovoltaic materials: Present efficiencies and future challenges. *Science* **2016**, *352*, aad4424.

(6) Bailie, C. D.; Christoforo, M. G.; Mailoa, J. P.; Bowring, A. R.; Unger, E. L.; Nguyen, W. H.; Burschka, J.; Pellet, N.; Lee, J. Z.; Grätzel, M.; et al. Semi-transparent perovskite solar cells for tandems with silicon and CIGS. *Energy Environ. Sci.* **2015**, *8*, 956–963.

(7) Albrecht, S.; Saliba, M.; Correa Baena, J. P.; Lang, F.; Kegelmann, L.; Mews, M.; Steier, L.; Abate, A.; Rappich, J.; Korte, L.; et al. Monolithic perovskite/silicon-heterojunction tandem solar cells processed at low temperature. *Energy Environ. Sci.* **2016**, *9*, 81–88.

(8) Sargent, E. H. Infrared photovoltaics made by solution processing. *Nat. Photonics* **2009**, *3*, 325–331.

(9) Kamat, P. V. Quantum dot solar cells. Semiconductor nanocrystals as light harvesters. *J. Phys. Chem. C* **2008**, *112*, 18737–18753.

DOI: 10.1021/acsenergylett.6b00403
ACS Energy Lett. 2016, 1, 852–857

(10) Sargent, E. H. Colloidal quantum dot solar cells. *Nat. Photonics* **2012**, *6*, 133−135.
(11) Ip, A. H.; Kiani, A.; Kramer, I. J.; Voznyy, O.; Movahed, H. F.; Levina, L.; Adachi, M. M.; Hoogland, S.; Sargent, E. H. Infrared colloidal quantum dot photovoltaics via coupling enhancement and agglomeration suppression. *ACS Nano* **2015**, *9*, 8833−8842.
(12) Atwater, H. A.; Polman, A. Plasmonics for improved photovoltaic devices. *Nat. Mater.* **2010**, *9*, 205−213.
(13) Yablonovitch, E.; Cody, G. D. Intensity enhancement in textured optical sheets for solar cells. *IEEE Trans. Electron Devices* **1982**, *29*, 300−305.
(14) Labelle, A. J.; Thon, S. M.; Kim, J. Y.; Lan, X.; Zhitomirsky, D.; Kemp, K. W.; Sargent, E. H. Conformal fabrication of colloidal quantum dot solids for optically enhanced photovoltaics. *ACS Nano* **2015**, *9*, 5447−5453.
(15) Aqoma, H.; Barange, N.; Ryu, I.; Yim, S.; Do, Y. R.; Cho, S.; Ko, D.-H.; Jang, S.-Y. Simultaneous Improvement of Charge Generation and Extraction in Colloidal Quantum Dot Photovoltaics Through Optical Management. *Adv. Funct. Mater.* **2015**, *25*, 6241−6249.
(16) Behaghel, B.; Tamaki, R.; Vandamme, N.; Watanabe, K.; Dupuis, C.; Bardou, N.; Sodabanlu, H.; Cattoni, A.; Okada, Y.; Sugiyama, M.; et al. Absorption enhancement through Fabry-Pérot resonant modes in a 430 nm thick InGaAs/GaAsP multiple quantum wells solar cell. *Appl. Phys. Lett.* **2015**, *106*, 081107.
(17) Brongersma, M. L.; Cui, Y.; Fan, S. Light management for photovoltaics using high-index nanostructures. *Nat. Mater.* **2014**, *13*, 451−460.
(18) Lee, K.-T.; Fukuda, M.; Joglekar, S.; Guo, L. J. Colored, see-through perovskite solar cells employing an optical cavity. *J. Mater. Chem. C* **2015**, *3*, 5377−5382.
(19) Sergeant, N. P.; Hadipour, A.; Niesen, B.; Cheyns, D.; Heremans, P.; Peumans, P.; Rand, B. P. Design of transparent anodes for resonant cavity enhanced light harvesting in organic solar cells. *Adv. Mater.* **2012**, *24*, 728−732.
(20) Song, H.; Guo, L.; Liu, Z.; Liu, K.; Zeng, X.; Ji, D.; Zhang, N.; Hu, H.; Jiang, S.; Gan, Q. Nanocavity enhancement for ultra-thin film optical absorber. *Adv. Mater.* **2014**, *26*, 2737−2743.
(21) Thompson, N. J.; Congreve, D. N.; Goldberg, D.; Menon, V. M.; Baldo, M. A. Slow light enhanced singlet exciton fission solar cells with a 126% yield of electrons per photon. *Appl. Phys. Lett.* **2013**, *103*, 263302.
(22) Gilot, J.; Barbu, I.; Wienk, M. M.; Janssen, R. A. The use of ZnO as optical spacer in polymer solar cells: theoretical and experimental study. *Appl. Phys. Lett.* **2007**, *91*, 113520.
(23) Green, M. A.; Keevers, M. J. Optical properties of intrinsic silicon at 300 K. *Prog. Photovoltaics* **1995**, *3*, 189−192.
(24) Ünlü, M. S.; Strite, S. Resonant cavity enhanced photonic devices. *J. Appl. Phys.* **1995**, *78*, 607−639.
(25) Pedrotti, F. L.; Pedrotti, L. S. *Introduction to Optics*, 2nd ed.; Prentice Hall, 1993; Vol. *1*.
(26) Orfanidis, S. J. *Electromagnetic Waves and Antennas*; Rutgers University, 2016; Chapter 6-Multilayer Structures, pp 185−204.
(27) Burkhard, G. F.; Hoke, E. T.; McGehee, M. D. Accounting for interference, scattering, and electrode absorption to make accurate internal quantum efficiency measurements in organic and other thin solar cells. *Adv. Mater.* **2010**, *22*, 3293−3297.
(28) Blech, M.; Laades, A.; Ronning, C.; Schröter, B.; Borschel, C.; Rzesanke, D.; Lawerenz, A. *Detailed study of PECVD silicon nitride and correlation of various characterization techniques*. Proceedings of the 24th European Photovoltaic Solar Energy Conference and Exhibition, Hamburg, Germany; 2009; pp 507−511.
(29) Wan, Y.; McIntosh, K. R.; Thomson, A. F. Characterisation and optimization of PECVD SiNx as an antireflection coating and passivation layer for silicon solar cells. *AIP Adv.* **2013**, *3*, 032113.
(30) Liu, M.; de Arquer, F.; Li, Y.; Lan, X.; Kim, G.-H.; Voznyy, O.; Jagadamma, L. K.; Abbas, A. S.; Hoogland, S.; Lu, Z.; et al. Double-Sided Junctions Enable High-Performance Colloidal-Quantum-Dot Photovoltaics. *Adv. Mater.* **2016**, *28*, 4142−4148.
(31) Zhitomirsky, D.; Voznyy, O.; Levina, L.; Hoogland, S.; Kemp, K. W.; Ip, A. H.; Thon, S. M.; Sargent, E. H. Engineering colloidal quantum dot solids within and beyond the mobility-invariant regime. *Nat. Commun.* **2014**, *5*, 3803.
(32) Hines, M. A.; Scholes, G. D. Colloidal PbS nanocrystals with size-tunable near-infrared emission: observation of post-synthesis self-narrowing of the particle size distribution. *Adv. Mater.* **2003**, *15*, 1844−1849.
(33) Lan, X.; Voznyy, O.; García de Arquer, F. P.; Liu, M.; Xu, J.; Proppe, A. H.; Walters, G.; Fan, F.; Tan, H.; Liu, M.; Yang, Z.; Hoogland, S.; Sargent, E. H. 10.6% Certified Colloidal Quantum Dot Solar Cells via Solvent-Polarity-Engineered Halide Passivation. *Nano Lett.* **2016**, *16*, 4630−4634.

DOI: 10.1021/acsenergylett.6b00403
ACS Energy Lett. 2016, 1, 852−857